OPTICAL COHERENCE TOMOGRAPHY IMAGE DENOISING USING SSR AND NON-LOCAL MEANS

S.Savitha Priyanka[1], Dr. P.Sivakumar[2]
[1]PG Scholar, [2]Associate Professor&Head/ECE, M.E., Ph.D
GRT Institute of Engineering and Technology, Tiruttani, India.

ABSTRACT: We demonstrate the usefulness of utilizing a segmentation step for improving the performance of sparsity based image reconstruction algorithms. In specific, we will focus on retinal optical coherence tomography (OCT) reconstruction and propose a novel segmentation based reconstruction framework with sparse representation, termed segmentation based sparse reconstruction (SSR). The SSR method uses automatically segmented retinal layer information to construct layer-specific structural dictionaries. In addition, the SSRmethod efficiently exploits patch similarities within each segmented layer to enhance the reconstruction performance. Our experimental results on clinical-grade retinal OCT images demonstrate the effectiveness and efficiency of the proposed SSR method for both denoising and interpolation of OCT images.

I. INTRODUCTION
MELANOMAS
The Four Basic Types Melanomas fall into four Optical coherence tomography (OCT) is a non-invasive imaging modality which is employed in diverse medical applications especially for diagnostic ophthalmology. Automated remote analysis of ophthalmologic OCT images is becoming more prevalent for the diagnosis and study of ocular diseases [3]. However, sample-based speckle and detector noise corrupts OCT images. On another front, to accelerate the acquisition process, relatively low spatial sampling rate is often used in capturing clinical OCT images. Both the heavy noise and low spatial sampling rate negatively affect automated and even manual OCT image analysis performance, necessitating utilization of effective denoising and interpolation techniques, respectively. Denoising and interpolation are two well-known reconstruction problems in the image processing. In the past decade, various models have been proposed to reconstruct high quality OCT images for various applications. In the context of biomedical imaging analysis and computer-assisted diagnosis, segmentation analysis is an intense field of research and development. The most difficult part of medical image analysis is the automated localization and delineation of structures of interest. Automated data evaluation is one way of enhancing the clinical utility of measurements. In particular, medical image segmentation extracts meaningful information and facilitate the display of this information in a clinically relevant way. A crucial role for automated information extraction in medical imaging usually involves the segmentation of regions of the image in order to quantify volumes and areas of interest of biological tissues for further diagnosis and localization of pathologies. Optical coherence tomography (OCT) is a

powerful imaging modality used to image various aspects of biological tissues, such as structural information, blood flow, elastic parameters, change of polarization states and molecular content (Huang et al., 1991). OCT uses the principle of low coherence interferometry to generate two or three dimensional imaging of biological samples by obtaining high-resolution cross-sectional backscattering profiles. A variety of successful algorithms for computer-aided diagnosis by means of OCT image analysis are presented in the literature, but robust use in clinical practice is still a major challenge for ongoing research in OCT image analysis. There are, therefore, efforts being made to improve clinical decision making based on automated analysis of OCT data. Particularly, in ophthalmology, efforts have been made to characterize clinically important features, such as damage to the fovea and optic nerve, automatically. The transfer of image analysis models from algorithmic development into clinical application is currently the major bottleneck due to the complexity of the overall process. For example, the process to establish an application for OCT medical image analysis requires difficult and complex tasks that should considers the following actions: 1) to define the OCT image data structures representing relevant biomedical features and the algorithms determining a valid example for given image values, 2) to select meaningful values for all technical parameters of the image data structures and algorithms and, as a result, to configure such a method to operate on specific OCT clinical data, 3) to run the algorithm with the selected parameters to find the individual model instance that best explains the input image and 4) to validate the procedure to ensure a trustworthy result from an automated segmentation algorithm even if a gold standard is unavailable.

II. RELATED WORKS
Fast Acquisition and Reconstruction of Optical Coherence Tomography Images via Sparse Representation
Present a novel technique, based on compressive sensing principles, for reconstruction and enhancement of multi-dimensional image data. Our method is a major improvement and generalization of the multi-scale sparsity based tomographic denoising (MSBTD) algorithm we recently introduced for reducing speckle noise. Our new technique exhibits several advantages over MSBTD, including its capability to simultaneously reduce noise and interpolate missing data.

Automated Mosaicing of Feature-Poor Optical Coherence Tomography Volumes With an Integrated White Light

Imaging System
Demonstrate the first automated, volumetric mosaicing algorithm for optical coherence tomography (OCT) that both accommodates 6-degree-of-freedom rigid transformations and implements a bundle adjustment step amenable to generating large fields of view with endoscopic and freehand imaging systems. Our mosaicing algorithm exploits the known, rigid connection between a combined white light and OCT imaging system to reduce the computational complexity of traditional volumetric mosaicing pipelines.

Automated 3-D Retinal Layer Segmentation of Macular Optical Coherence Tomography Images With Serous Pigment Epithelial Detachments
Automated retinal layer segmentation of optical coherence tomography (OCT) images has been successful for normal eyes but becomes challenging for eyes with retinal diseases if the retinal morphology experiences critical changes. We propose a method to automatically segment the retinal layers in 3-D OCT data with serous retinal pigment epithelial detachments (PED), which is a prominent feature of many chorioretinal disease processes.

Current retinal imaging modalities Millions of people worldwide live with retinal disease and the accompanying threat of severe vision loss or blindness. During the last few years, the retinal research field has undergone a dramatic change in terms of diagnostic tools and therapies that have resulted in substantial benefits for patients suffering from retinal disease. Traditionally the retina has been observed either directly via an ophthalmoscope or similar optical devices such as the fundus camera. The field of ophthalmology was revolutionized in 1851 with the invention of the ophthalmoscope by Hermann von Helmholtz (von Helmholtz, 1851) as for the first time detailed examinations of the interior of the eye could be made in living patients.

III. EXISTING METHOD
The emergence of ultrabroad bandwidth femtosecond laser technology has allowed the development of an ultra-high resolution OCT, which has been demonstrated to achieve axial resolutions of 3 μm during in vivo imaging of the human retina, which is two orders of magnitude higher than what can be achieved by conventional ultrasound imaging. Figure 6 shows the ultrahigh resolution OCT cross section of a normal human macula showing all of the major layers and internal structures of the retina. The ultrahigh resolution OCT will in effect be a microscope capable of revealing certain histopathological aspects of macular disease in the living eye. As it was previously explained, in the conventional or time domain OCT (TDOCT) system the length of the reference arm in an interferometer is rapidly scanned over a distance corresponding to the imaging depth range. The mechanism of scanning largely limits the acquisition speed and makes real-time imaging impossible. In recent years a new model OCT based on Fourier domain interferometry has emerged, and it has been called spectral domain OCT (SDOCT) or Fourier domain OCT (FDOCT) (Fercher et al., 1995; Fercher et al., 2003; Hausler & Lindner, 1998). SDOCT can avoid scanning

of the reference, thus it can reach very high acquisition speed. As a matter of fact, in time domain OCT the location of scatters in the sample is observed by generation of interferometric fringes at the detector as the reference reflector position is axially translated. In contrast, Fourier domain OCT required the reference arm to be held fixed, and the optical path length difference between sample and reference reflections is encoded by the frequency of the interferometric fringes as a function of the source spectrum.

IV. PROPOSED SYSTEM
The wave front reconstruction is formulated as an inverse problem where the complex exponent or the amplitude and phase of this exponent are assumed to admit sparse representations in suitable scarifying transforms (dictionaries). The sparse modeling is a form of regularization of the inverse problem. For design of these overcomplete scarifying dictionaries we use Block matching 3D (BM3D) and learning dictionary techniques. Various optical setups (interferometric and non-interferometric) are considered with algorithms developed for Gaussian and Poisoning noise in intensity measurements.
Segmentation based sparse reconstruction (SSR) model to develop a fast and accurate reconstruction algorithm. Then, for each layer, SSR constructs a dedicated structural dictionary to better represent the anatomic and pathologic structures within this layer. Finally, instead of searching the whole image, SSR efficiently searches for the similar patches within each layer and exploits the patches' similarities within each layer to improve the sparse decomposition.

Nonlocal Means Reconstruction Model
For the image denoising and interpolation problems, another very effective reconstruction model is the nonlocal means, which exploits the self-similarities inherent to images. In the sparse reconstruction model, the sparse coefficient estimations are affected by the noise in observation image, thus leading to suboptimal reconstruction.To suppress noise interference, recent works including incorporate the nonlocal means into the sparse reconstruction model. Specifically, the nonlocal sparse model first conducts the similar patch search in the whole image and then jointly exploits correlations among similar patches by decomposing them on the same atoms of the dictionary to improve the sparse coefficient solution.

MODULES DESCRIPTION
The SSR method, which utilizes the layer specific structural information to enhance the effectiveness and cost efficiency of our previous sparse reconstruction techniques. The SSR method is composed of three main parts:
a) layer segmentation
b) layer segmentation based dictionary construction
c) layer segmentation based sparse reconstruction.

LAYER SEGMENTATION
For all the testing and training retinal images, we utilize the popular graph theory and dynamic programming (GTDP) method to automatically segment these images into R layers

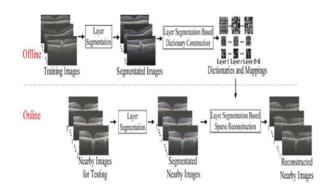Layer Segmentation Based Dictionary Construction
In the retinal OCT image, different layers contain various types of anatomic and pathologic structures (e.g., vessels, drusen, edema, and fovea), and different thicknesses and speckle structures.Therefore, to well represent complex structures in varied layers, we utilize the segmented layer information to train multiple structural dictionaries (each corresponding to one layer), rather than one general dictionary.

Layer Segmentation Based Sparse Reconstruction
As noted, the anatomic and pathologic structures, intensities, and speckle patterns within each layer are expected to have strong similarities. Therefore, instead of searching the whole image.Proposed to seek the similar patches in a searching window within each segmented layer, which can greatly reduce the search space.

Joint Sparse Reconstruction for Denoising
In denoising, simultaneous decomposition of the nearby averaged Patches in the r -th layer of nearby images with the joint sparse technique amounts
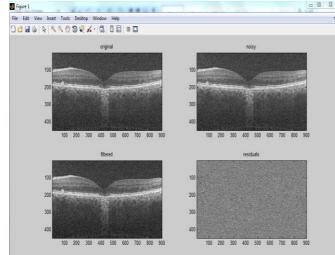

V. RESULTS AND DISCUSSIONS

Figure 5.1 shows the Noisy Image with an under sampling factor of 5. Shows the original images and noise generated image and filtered image and last image is residual of the difference image between the reference image with filtered images are shown at the right of each denoised image
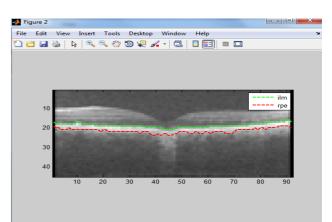

Figure 5.2 SSR reconstruction results using two different layer segmentations.

To artificially create more severe segmentation errors, we intentionally introduced errors in segmentation of the inner nuclear layer in the black box region (manually induced error), resulting in the images .

The next step is Image Filtering. By using SRAD, Lee, Kaun and Wavelet Denoising the Image Filtering Can be done.

COMPARISION TABLE FOR ALL FILTERS

After Filter the Image Quality Measure (PSNR, MSE, NCC, NAE) Can be calculated between the original image and filtered image.

Peak Signal to Noise Ratio (PSNR):
$$PSNR(I,\hat{I}) = 10\log\left(\frac{\max(I^2)}{MSE(I,\hat{I})}\right)$$

Mean Squared Error (MSE):
$$MSE(I,\hat{I}) = \frac{1}{NM}\sum_{i=1}^{N}\sum_{j=1}^{M}\left(I_{i,j} - \hat{I}_{i,j}\right)^2$$

Normalized Absolute Error (NAE):
$$NAE(I,\hat{I}) = \frac{\sum_{i=1}^{N}\sum_{j=1}^{M}|I_{i,j} - I_{i,j}|}{\sum_{i=1}^{N}\sum_{j=1}^{M}|I_{i,j}|}$$

Normalized Cross-Correlation (NCC):
$$NCC(I,\hat{I}) = \frac{\sum_{i=1}^{N}\sum_{j=1}^{M}(I_{i,j} \cdot I_{i,j})}{\sum_{i=1}^{N}\sum_{j=1}^{M}(I_{i,j})^2}$$
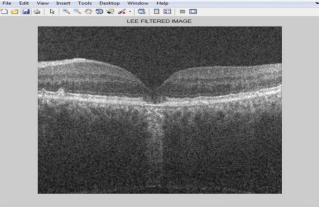

Figure 5.3 Shows the LEE filtered Image

A Lee filter using MATLAB for despeckling of an image. Since it's a patch based processing, the computation cost will be high.

This function takes the reference image, speckled/noisy image and the window size as input and performs the following steps.

1.   The variance of the reference image is found. Variance can be found either by using MATLAB built-in function or user defined function. Here in this case, a user defined function is used to find the variance.

2.   Based on the size of the kernel, the noisy image is padded with zeros on all sides.

3.   The center index of the kernel is found

4.   The noisy image is processed patch by patch.

Figure 5.4 Shows the KUAN Filter Image

Kuan filter were the earliest filters working directly on the intensity of the image using local statistics and is based on the minimum mean square error (MMSE), which produce the speckle free image governed by the relationship
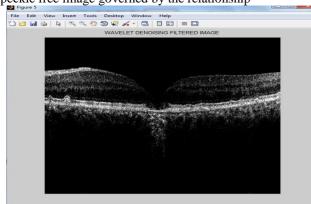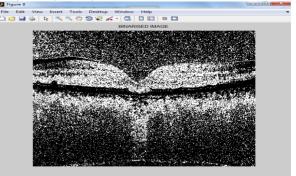

Figure 5.5 Shows the Wavelet Denoising Filter Image

To denoise signals and images. Because wavelets localize features in your data to different scales, you can preserve important signal or image features while removing noise. The basic idea behind wavelet denoising, or wavelet thresholding, is that the wavelet transform leads to a sparse representation for many real-world signals and images. What this means is that the wavelet transform concentrates signal and image features in a few large-magnitude wavelet coefficients. Wavelet coefficients which are small in value are typically noise and you can "shrink" those coefficients or remove them without affecting the signal or image quality. After you threshold the coefficients, you reconstruct the data using the inverse wavelet transform.

	LEE	KUAN	WAVELET	SRAD
PSNR	29.1710	29.9502	8.0144	47.3118
MSE	78.7010	65.7751	1.0272e+04	1.2075
NCC	0.9841	0.9839	6.4033e-04	0.2604
NAE	0.0747	0.0691	0.9996	0.7506

This figure 5.6 shows the Quality measures from denoised to original image.

Classification models in machine learning are evaluated for their performance by common performance measures. This function calculates the following performance measures PSNR , MSE , NAE , NCC

This figure 5.7 shows the Binaries Image.

BW = im2bw(I,level) converts the grayscale image I to binary image BW, by replacing all pixels in the input image with luminance greater than level with the value 1(white) and replacing all other pixels with the value 0 (black).

This range is relative to the signal levels possible for the image's class. Therefore, a level value of 0.5 corresponds to an intensity value halfway between the minimum and maximum value of the class.
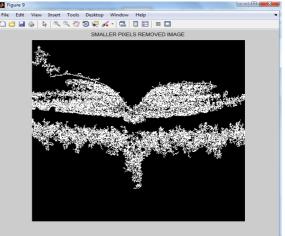

Fig 5.8 SMALLER PIXELS REMOVED IMAGE

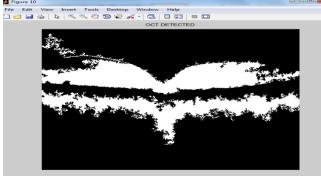Next step is smaller filer image using Image Morphological operators. Final Step is thickness detection.

Fig .5.9 Impact of SSR reconstruction on automatic layer segmentation performance.

SSR denoised image using the segmentation results. Automatic segmentation of the image Thresholding technique is shown, where the accuracy of segmentation is improved for the previous erroneously segmented region.

EXISTING SYSTEM

```
    MSE:    1.21

    PSNR: 47.2884842 dB
progress: 10% done, this may take a while...

progress: 20% done, this may take a while...

progress: 30% done, this may take a while...

progress: 40% done, this may take a while...

progress: 50% done, this may take a while...

progress: 60% done, this may take a while...

progress: 70% done, this may take a while...

progress: 80% done, this may take a while...

progress: 90% done, this may take a while...

progress: 100% done, this may take a while...

Elapsed time is 104.518766 seconds.
```

This figure 5.8 shows the Quality measures from denoised to original image.

PROPOSED SYSTEM

```
SRAD FILTER


ans =


PSNR is 47.311829 dB



ans =


THICKNESS is 5.106452 mm


Elapsed time is 72.357425 seconds.
```

This figure 5.9 shows the Quality measures from denoised to original image.

TABULTATION

IMAGE NAME	EXISTING SYSTEM		PROPOSED SYSTEM	
	TIME	PSNR	TIME	PSNR
1.tif	104.51	47.28	72.35	47.31
2.tif	108.44	47.273	74.83	47.295
3.tif	102.97	47.28	67.15	47.295
4.tif	106.77	47.32	72.72	47.391

Table 5.1 Shows the Performance Comparison of Existing and Proposed Method

VI. CONCLUSION

In contrast to OCT technology development which has been a field of active research since 1991, OCT image segmentation has only being fully active explored during the last decade. However, it continues to be one of the more difficult and at the same time most commonly required steps in OCT image analysis, therefore, there does not and can not exist a typical segmentation method that can be expected to work equally well for all tasks. The works cited in this review spread from the 1997's until September 2010. Of course, the citation in this review is by no means complete. For example, an early active research topic such as manual tools for image segmentation has not been covered. It is also worthy the mentioning that it was difficult to assess the robustness of the various segmentation approaches because of many authors have used different OCT imaging setups and reported limited quantitative.

REFERENCES

[1] D. Huang et al., "Optical coherence tomography," Science, vol. 254, no. 5035, pp. 1178–1181, Nov. 1991.

[2] S. Bhat, I. V. Larina, K. V. Larin, M. E. Dickinson, and M. Liebling, "4D reconstruction of the beating embryonic heart from two orthogonal sets of parallel optical coherence tomography slice-sequences," IEEE Trans. Med. Imag., vol. 32, no. 3, pp. 578–588, Mar. 2013.

[3] F. Shi et al., "Automated 3-D retinal layer segmentation of macular optical coherence tomography images with serous pigment epithelial detachments," IEEE Trans. Med. Imag., vol. 34, no. 2, pp. 441–452, Feb. 2015.

[4] L. Fang et al., "Fast acquisition and reconstruction of optical coherence tomography images via sparse representation," IEEE Trans. Med. Imag., vol. 32, no. 11, pp. 2034–2049, Nov. 2013.

[5] M. D. Robinson, S. J. Chiu, C. A. Toth, J. Izatt, J. Y. Lo, and S. Farsiu, "Novel applications of super-resolution in medical imaging," in Super-Resolution Imaging, P. Milanfar, Ed. Boca Raton, FL, USA: CRC Press, 2010, pp. 383–412.

[6] R. Kafieh, H. Rabbani, and I. Selesnick, "Three dimensional data-driven multi scale atomic tepresentation of optical coherence tomography," IEEE Trans. Med. Imag., vol. 34, no. 5, pp. 1042–1062, May 2015.

[7] P. Milanfar, "A tour of modern image filtering:

New insights and methods, both practical and theoretical," IEEE Signal Process. Mag., vol. 30, no. 1, pp. 106–128, Jan. 2013.

[8] H. M. Salinas and D. C. Fernandez, "Comparison of PDE-based nonlinear diffusion approaches for image enhancement and denoising in optical coherence tomography," IEEE Trans. Med. Imag., vol. 26, no. 6, pp. 761–771, Jun. 2007.

[9] A. Ozcan, A. Bilenca, A. E. Desjardins, B. E. Bouma, and G. J. Tearney, "Speckle reduction in optical coherence tomography images using digital filtering," J. Opt. Soc. Am., vol. 24, no. 7, pp. 1901–1910, Jul. 2007.

[10] A. Wong, A. Mishra, K. Bizheva, and D. A. Clausi, "General Bayesian estimation for speckle noise reduction in optical coherence tomography retinal imagery," Opt. Exp., vol. 18, no. 8, pp. 8338–8352, Apr. 2010.

[11] A. Boroomand, A. Wong, E. Li, D. S. Cho, B. Ni, and K. Bizheva, "Multi-penalty conditional random field approach to super-resolved reconstruction of optical coherence tomography images," Biomed. Opt. Exp., vol. 4, no. 10, pp. 2032–2050, Apr. 2013.

[12] X. Liu and J. U. Kang, "Compressive SD-OCT: The application of compressed sensing in spectral domain optical coherence tomography," Opt. Exp., vol. 18, no. 21, pp. 22010–22019, Oct. 2010.

[13] D. Xu, N. Vaswani, Y. Huang, and J. U. Kang, "Modified compressive sensing optical coherence tomography with noise reduction," Opt. Lett., vol. 37, no. 20, pp. 4209–4211, Aug. 2012.

[14] D. Xu, Y. Huang, and J. U. Kang, "Real-time compressive sensing spectral domain optical coherence tomography," Opt. Lett., vol. 39, no. 1, pp. 76–79, Jan. 2014.

[15] E. Lebed, P. J. Mackenzie, M. V. Sarunic, and F. M. Beg, "Rapid volumetric OCT image acquisition using compressive sampling," Opt. Exp., vol. 18, no. 20, pp. 21003–21012, Aug. 2010.

[16] A. B. Wu, E. Lebed, M. V. Sarunic, and M. F. Beg, "Quantitative evaluation of transform domains for compressive sampling-based recovery of sparsely sampled, volumetric OCT images," IEEE Trans. Biomed. Eng., vol. 60, no. 2, pp. 470–478, Feb. 2013.

[17] K. L. Lurie, R. Angst, and A. K. Ellerbee, "Automated mosaicing of feature-poor optical coherence tomography, volumes with an integrated white light imaging system," IEEE Trans. Biomed. Eng., vol. 61, no. 7, pp. 2141–2153, 2014.

[18] H. Rabbani, R. Nezafat, and S. Gazor, "Wavelet-domain medical image denoising using bivariate Laplacian mixture model," IEEE Trans. Biomed. Eng., vol. 56, no. 12, p. 2826, Dec. 2009.

[19] S. Chitchian, M. A. Fiddy, and N. M. Fried, "Denoising during optical coherence tomography of the prostate nerves via wavelet shrinkage using dual-tree complex wavelet transform," J. Biomed. Opt., vol. 14, no. 1, p. 014031-6, Jan. 2009.

[20] Z. Jian, L. Yu, B. Rao, B. J. Tromberg, and Z. Chen, "Threedimensional speckle suppression in optical coherence tomography based on the curvelet transform," Opt. Exp., vol. 18, no. 2, pp. 1024–1032, Jan. 2010.